

On the evolution of a fossil disk around neutron stars originating from merging WDs

Bai Sheng Liu^{1,2} and Xiang-Dong Li^{1,2}

¹*Department of Astronomy, Nanjing University, Nanjing 210046, China*

²*Key laboratory of Modern Astronomy and Astrophysics (Nanjing University), Ministry of Education, Nanjing 210046, China*

lixd@nju.edu.cn

ABSTRACT

Numerical simulations suggest that merging double white dwarfs (WDs) may produce a newborn neutron star surrounded by a fossil disk. We investigate the evolution of the fossil disk following the coalescence of double WDs. We demonstrate that the evolution can be mainly divided into four phases: the slim disk phase (with time $\lesssim 1$ yr), the inner slim plus outer thin disk phase ($\sim 10 - 10^6$ yr), the thin disk phase ($\sim 10^2 - 10^7$ yr), and the inner advection-dominated accretion flow plus outer thin disk phase, given the initial disk mass $\sim 0.05 - 0.5 M_\odot$ and the disk formation time $10^{-3} - 1$ s. Considering possible wind mass loss from the disk, we present both analytic formulae and numerically calculated results for the disk evolution, which is sensitive to the condition that determines the location of the outer disk radius. The systems are shown to be very bright in X-rays in the early phase, but quickly become transient within $\lesssim 100$ yr, with peak luminosities decreasing with time. We suggest that they might account for part of the very faint X-ray transients around the Galactic center region, which generally require a very low mass transfer rate.

Subject headings: accretion, accretion disks—stars: evolution—stars: neutron—white dwarfs—X-rays: binaries

1. Introduction

White dwarfs (WDs) are the most common stellar remnants in the universe. Within 20 pc of the Solar system, about 25% of the WD population are in binary systems, and $\sim 6\%$ of them are double WDs (Holberg et al. 2008). WDs in compact binaries are responsible for

lots of interesting astrophysical phenomena. For example, due to the gravitational radiation, the double degenerate stars will gradually lose their orbital angular momenta and undergo a merging process at last. Thus, the coalescence of double WDs is a good source of strong gravitational wave radiation (e.g., [Fryer et al. 2002](#); [Ott 2009](#); [Yu & Jeffery 2010](#); [Kilic et al. 2014](#)).

The merger remnants of double WDs can be various kinds of exotic objects, depending on the merging process and the initial conditions of the WDs including the total WD masses ([van Kerkwijk et al. 2010](#); [van Kerkwijk 2013](#)), the binary mass ratio, the synchronization timescale (e.g., [Zhu et al. 2013](#)), and the mass loss during the merging events (e.g., [Dessart et al. 2006](#); [Dan et al. 2011](#); [Raskin & Kasen 2013](#)). If the remnant mass is less than the Chandrasekhar mass limit (M_{Ch}), the outcome may be a sdB/sdO star (e.g., [Saio & Jeffery 2000](#); [Han et al. 2002](#); [Heber 2009](#)), or a R Coronae Borealis star (e.g., [Webbink 1984](#); [Jeffery et al. 2011](#); [Longland et al. 2011](#); [Zhang et al. 2014](#)). This merger scenario has been proposed to explain the bright, massive ($\gtrsim 0.8 M_{\odot}$) WDs in the Galactic halo (e.g., [Yuan 1992](#); [Liebert et al. 2005](#)), the existence of a disk around a WD with a metal-rich atmosphere (e.g., [García-Berro et al. 2007](#)), and WDs with a strong (around 10^{6-9} G) magnetic field (e.g., [García-Berro et al. 2012](#); [Külebi et al. 2013](#)).

If the merger remnant is more massive than M_{Ch} , the system is expected to either explode as a Type Ia supernova (SN Ia, [Webbink 1984](#); [Iben & Tutukov 1984](#)), or collapse to a neutron star (NS) (i.e., accretion-induced collapse or AIC, [Saio & Nomoto 1985](#); [Rueda et al. 2013](#))¹. During the merger of double WDs, both mass and angular momentum are accreted onto the more massive WD. In the AIC case, the newborn NS, may be rapidly rotating and behave as a normal pulsar (PSR) or a millisecond pulsar (MSP; e.g., [Bhattacharya & van den Heuvel 1991](#)). Moreover, if the magnetic field of the progenitor is strong enough, it may be amplified via dynamo action and flux conservation during the collapse ([Duncan & Thompson 1992](#)), and hence the end product could be a magnetar (e.g., [Usov 1992](#); [King et al. 2001](#); [Levan et al. 2006](#)).

Both smoothed particle hydrodynamics ([Benz et al. 1990](#); [Yoon et al. 2007](#); [Lorén-Aguilar et al. 2009](#)) and grid-based techniques ([D’Souza et al. 2006](#); [Motl et al. 2007](#)) have been adopted to investigate the coalescence processes of double WDs. A delayed explosion is generally observed. The less massive WD is disrupted, and a hot, rotating corona, surrounded by a thick disk, forms around the more massive WD. The outcome of the CO WD merger depends on whether the C-ignition occurs at the center ([Saio & Nomoto 1985, 1998, 2004](#))

¹Note that besides the above double degenerate model, the single degenerate one ([Whelan & Iben 1973](#); [Nomoto & Kondo 1991](#)) is another route to produce the above events.

or in the envelope of the accreting WD (Nomoto & Iben 1985), which may be determined by the accretion rate (Nomoto & Iben 1985; Kawai et al. 1987). If the ignition occurs at the center, a SN Ia will follow, provided that the accretion rate is less than $2.7 \times 10^{-6} M_{\odot} \text{ yr}^{-1}$. If the C-burning starts from the outer layer, the object will collapse to be a NS.

According to numerical simulations of WD mergers leading to AIC (Dessart et al. 2006, 2007), a fossil disk of mass $\sim 0.05 - 0.5 M_{\odot}$ is left around the newborn NS. Metzger et al. (2009b) calculated the evolution of the composition of the accretion disk, and found that no other intermediate-mass elements are synthesized unlike SN Ia events, and strong winds blow away some disk mass containing $\sim 10^{-2} M_{\odot}$ ^{56}Ni , which may explain some sub-luminous SN Ia events. Darbha et al. (2010) showed that the light curves and spectra may help distinguish the WD merging events from other transient events, e.g., Ia and binary NS mergers.

In this work we focus on the evolution of the fossil disks around the NSs following the WD coalescence, which is similar to that of supernova fallback disks (e.g., Menou et al. 2001; Shen & Matzner 2012). While most of the previous studies pay attention to the disk evolution at the early, bright stage, our work extends the evolution to the late, faint phase. In addition, we consider the influence on the disk evolution of both neutrality in the disk and self-gravity of the disk, which are seldom noticed in previous studies.

This paper is organized as follows. We model the evolution of the fossil disk around a NS following an AIC event in Section 2. Section 3 presents numerically calculated results based on the model parameters. We discuss the possible observational implications of the fossil disk model in Section 4 and summarize in Section 5.

2. The Model

Although the evolution of the fossil disks in the AIC model is still under discussion, the studies on the evolution of the fallback disks originating from tidal disruption events (TDEs) and SNe could be good references, as illustrated by their similar formation processes. During a TDE, as a star is tidally disrupted by a supermassive black hole, roughly half of its debris falls back and orbits the black hole, gradually forms a disk and accretes onto the hole (e.g., Rees 1988). When a NS is produced in the SN explosion, the progenitor’s envelope is ejected outwards; part of the ejecta may be gravitationally captured by the NS and form a fallback disk around it if there is sufficient angular momentum (e.g., Michel 1988; Chevalier 1989). In the AIC scenario, during the coalescence of double WDs, a fossil disk or torus, which originates from the disrupted, less massive WD, is also observed to be left over around the newborn NS (e.g., Saio & Nomoto 2004; Dessart et al. 2006). Therefore the evolution of

these fossil disks is likely to follow similar rules. The whole evolution can be divided into the following four phases. (i) In phase 1, the whole, newly formed disk is geometrically slim or even thick with a super-Eddington accretion rate, where advection dominates cooling (e.g., [Cannizzo & Gehrels 2009](#)). (ii) In phase 2, along with the decrease of the accretion rate and the expansion of the disk, the outer part of the disk gradually turns to be geometrically thin, where radiative cooling becomes effective, that is, the disk contains an inner slim region and an outer thin region, with the latter advancing inward. (iii) In phase 3, the whole disk becomes optically thick and geometrically thin. (iv) In phase 4, the inner region of the disk begins to become advection-dominated accretion flow (ADAF) where radiative cooling is inefficient, which is surrounded by a outer thin disk. The ADAF region develops outwards with decreasing accretion rate.

In the following we discuss the disk evolution in detail.

2.1. Initial Parameters

We consider a NS with mass $M = 1.4 M_{\odot}$ and radius $R_{\text{NS}} = 10^6$ cm. The accretion rate \dot{M} is expressed in units of the Eddington accretion rate \dot{M}_{Edd} , i.e., $\dot{m} = \dot{M}/\dot{M}_{\text{Edd}}$. Here $\dot{M}_{\text{Edd}} = 10L_{\text{Edd}}/c^2 = 1.39 \times 10^{18} m \text{ gs}^{-1}$ with $m = M/M_{\odot}$ and $L_{\text{Edd}} = 1.25 \times 10^{38} m \text{ erg s}^{-1}$. The interesting radius R in the disk is scaled with the Schwarzschild radius $R_{\text{S}} = 2GM/c^2 = 2.95 \times 10^5 m \text{ cm}$, i.e., $r = R/R_{\text{S}}$. The formation time t_{f} of the disk ranges from ~ 1.0 ms to 1.0 s, and the initial disk mass $M_{\text{D},0} = \eta M_{\odot}$ with $\eta = 0.05 - 0.5$, depending on the total mass, the initial mass ratio q , and the mass loss during AIC (e.g., [Dessart et al. 2006](#); [Dan et al. 2011](#); [Raskin & Kasen 2013](#); [Zhu et al. 2013](#)), etc. Generally smaller q (if $q < 1$) may lead to a larger $M_{\text{D},0}$ ([Metzger et al. 2008](#)). The mass distribution of the disk is very close to that of NS + NS or NS + black hole (BH) mergers (e.g., [Metzger et al. 2009a](#)), so the model may also be applicable to those cases.

The inner radius r_{i} and the outer radius r_{out} of the disk at t_{f} are assigned to be $r_{\text{i}} \gtrsim 2.5$ (roughly the radius of the newborn NS) and $r_{\text{out}} = r_{\text{f}} \sim 10^{3-4}$ (roughly the radius of the accreting WD), respectively. We assume that the NS magnetic field is very weak ($\lesssim 10^{8-9}$ G), so the disk can reach the surface of the NS. In the future work we will consider the interaction of a strong magnetic field with the disk. The outer disk spreads due to angular momentum transport ([Lynden-Bell & Pringle 1974](#); [Pringle 1991](#)), until it reaches a radius where self-gravity becomes important. The stability criterion for a differentially rotating disk is $Q \equiv \frac{c_{\text{s}} \Omega_{\text{K}}}{\pi G \Sigma} = 1$, where c_{s} , Ω_{K} , and Σ are the sound speed, the Keplerian angular velocity, and the surface density of the disk material, respectively, and G is the gravitational

constant (Toomre 1964). This defines the self-gravity radius as (Burderi et al. 1998),

$$r_{\text{sg}} \simeq 2.92 \times 10^5 \cdot m^{-2/3} \cdot \left(\frac{\rho}{1 \text{ g cm}^{-3}} \right)^{-1/3}, \quad (1)$$

where ρ is the density of the disk material. Note that the magnitude of the self-gravity radius is very similar to the Roche limit (e.g., Aggarwal & Oberbeck 1974; Menou et al. 2001), and we will see that it is a crucial factor in the disk evolution.

As the accretion rate decays, the energy dissipation rate in the disk decreases. The outermost disk, which is the coldest, will become neutral eventually once the temperature is lower than a critical value $T_{\text{P}} \sim 6500 \text{ K}$ (Menou et al. 2001; Ertan et al. 2009). After that there is hardly any transport of mass or angular momentum in the disk. However, it has been suggested the irradiation from the central source may prevent the appearance of a passive disk even at a lower temperature (Alpar 2001; Inotsuka & Sano 2005; Alpar et al. 2013). The disk evolution, after being neutral, is less certain and beyond our interest. In the following calculations, the outer disk is assumed to be neutral and unchanging if its temperature drops to $T_{\text{P}} = 300 \text{ K}$ (Alpar 2001).

2.2. Disk Evolution

After the coalescence of double WDs, a fossil disk originating from the ejecta is formed around the NS with a timescale $\sim 1.0 \text{ ms} - 1.0 \text{ s}$ (Dessart et al. 2006). Along with mass accretion, the disk spreads to a larger radius due to the conservation of angular momentum. The evolution of the surface density Σ of the fossil disk is governed by a linear, viscous diffusion equation (Pringle 1981; Cannizzo et al. 1990),

$$\frac{\partial \Sigma}{\partial t} = \frac{3}{R} \frac{\partial}{\partial R} \left[R^{1/2} \frac{\partial}{\partial R} (\nu \Sigma R^{1/2}) \right], \quad (2)$$

where $\nu = 2\alpha P / (3\rho\Omega_{\text{K}})$ is the kinetic viscosity coefficient. Here P is the pressure and α is the standard Shakura & Sunyaev (1973) viscosity parameter. If ν follows a power law of R , $\nu \propto R^n$, the above equation can be solved analytically with self-similarity solutions (Pringle et al. 1974; Pringle 1981). The evolution of the disk can be classified into the following phases.

In phase 1, the accretion rate is usually so high that the disk is described by a slim disk model, where radiation pressure dominates and advection can effectively consume most of the heat locally generated (Abramowicz et al. 1988). While the fallback rate evolves with time $\propto t^{-5/3}$ (Phinney 1989), the accretion rate linked to viscous diffusion follows $\propto t^{-4/3}$. Meanwhile, in the slim disk phase possible disk wind loss should be taken into account, so

the local accretion rate is assumed to follow a power law of the radius, $\dot{m}(r) \propto r^s$, where the power-law index s ($0 < s < 1$) is believed to be constant (Blandford & Begelman 1999; Narayan et al. 2001). If the wind loss is weak ($s < 1/3$), the accretion rate can be described by $\propto t^{-4/3-s}$, otherwise $\propto t^{-5/3}$ (Pringle 1991; Cannizzo & Gehrels 2009; Shen & Matzner 2012). Thus the parameters of the disk vary as,

$$\begin{aligned}\dot{m}(r, t) &= \begin{cases} \dot{m}_0 \left(\frac{r}{r_f}\right)^s \left(\frac{t}{t_f}\right)^{-4/3-s} & (0 < s < 1/3), \\ \dot{m}_0 \left(\frac{r}{r_f}\right)^s \left(\frac{t}{t_f}\right)^{-5/3} & (1/3 < s < 1), \end{cases} \\ r_{\text{out}}(t) &= r_f \left(\frac{t}{t_f}\right)^{2/3}, \\ T(r, t) &= T_0 \left(\frac{\dot{m}}{\dot{m}_0}\right)^{1/4} \left(\frac{r}{r_f}\right)^{-5/8}, \\ \rho(r, t) &= \rho_0 \left(\frac{\dot{m}}{\dot{m}_0}\right) \left(\frac{r}{r_f}\right)^{-3/2}, \end{aligned} \quad (3)$$

where T is the temperature, and the subscript 0 denotes variables measured at $t = t_f$ and $r = r_f$. From Cannizzo & Gehrels (2009) we have

$$\begin{aligned}T_0 &\simeq 1.0 \times 10^8 \left(\frac{\alpha m}{0.1}\right)^{-1/4} \dot{m}_0^{1/4} \cdot r_f^{-5/8} \text{ K}, \\ \rho_0 &\simeq 3.0 \times 10^{-4} \left(\frac{\alpha m}{0.1}\right)^{-1} \dot{m}_0 \cdot r_f^{-3/2} \text{ g cm}^{-3}, \end{aligned} \quad (4)$$

where \dot{m}_0 can be solved from the initial mass of the disk,

$$M_{\text{D},0} = \eta M_{\odot} = \dot{m}_0 \dot{M}_{\text{Edd}} t_f. \quad (5)$$

Phase 1 ends at the time t_1 when radiative cooling begins to dominate in the outermost region, that is, the transition radius r_{tra} , which separates the inner slim disk region from the outer radiative cooling-dominated region, starts to equal the outer disk radius. The slim disk region is characterized by both advective cooling and radiation pressure domination. The boundary condition for the slim-thin disk transition occurs when the ratio of the advective cooling and the energy generation via viscous dissipation becomes less than $1/3 - 1/2$ (e.g., Abramowicz et al. 1988; Kato et al. 1998). Detailed calculations show that advection starts to modify the disk structure at local accretion rates $\sim 0.6 - 0.8 \dot{M}_{\text{Edd}}$ (Watarai et al. 2000; Sadowski 2011). So we can roughly estimate r_{tra} as

$$r_{\text{tra}} \simeq \dot{m}(r_{\text{out}}, t) = r_{\text{out}}. \quad (6)$$

This yields

$$t_1 = \begin{cases} t_f \cdot \left(\frac{\dot{m}_0}{r_f}\right)^{3/(6+s)} & (0 < s < 1/3), \\ t_f \cdot \left(\frac{\dot{m}_0}{r_f}\right)^{3/(7-2s)} & (1/3 < s < 1). \end{cases} \quad (7)$$

In phase 2, The thin disk region develops inwards till the inner slim disk region disappears. While the inner slim disk region is always dominated by radiation pressure and electron scattering opacity, the outer thin disk region will undergo two status-transitions with decreasing accretion rate. Firstly, the outer, thin disk region, initially dominated by radiation pressure, gradually becomes supported by gas pressure. Secondly, the electron scattering opacity in the thin disk region is replaced by free-free absorption. The evolution can be separated by the time point t_{gas} when

$$r_{\text{gas}} \simeq 281 \cdot \left(\frac{\alpha m}{0.1}\right)^{2/21} \dot{m}^{16/21} = r_{\text{out}}, \quad (8)$$

where the radius r_{gas} separates the region dominated by gas pressure from that dominated by radiation pressure (Shakura & Sunyaev 1973).

Before the first status-transition ($t_1 < t < t_{\text{gas}}$), the whole disk comprises an inner, slim disk region and an outer, thin disk region (the entire disk is dominated by radiation pressure plus electron scattering opacity). Taking into account the fact that $\dot{m}(r) \propto r^s$ in the slim disk region and $\dot{m}(r) \propto t^{-8/7}$ in the thin disk region (Shen & Matzner 2012) and the boundary condition between them, one can obtain the following formulae for the disk evolution,

$$\begin{aligned} \dot{m}(r, t) &= \begin{cases} k_1 \left(\frac{t}{t_f}\right)^{-8(1-s)/7} \left(\frac{r}{r_f}\right)^s & \text{if } r_i < r < r_{\text{tra}}, \\ k_2 \left(\frac{t}{t_f}\right)^{-8/7} & \text{if } r_{\text{tra}} < r < r_{\text{out}}, \end{cases} \\ r_{\text{out}}(t) &= k_3 \left(\frac{t}{t_f}\right)^{2/7}, \\ T(r, t) &= \begin{cases} T_1 \left(\frac{\dot{m}}{\dot{m}_0}\right)^{1/4} \left(\frac{r}{r_f}\right)^{-5/8} & \text{if } r_i < r < r_{\text{tra}}, \\ T_2 \left(\frac{r}{r_f}\right)^{-3/4} & \text{if } r_{\text{tra}} < r < r_{\text{out}}, \end{cases} \\ \rho(r, t) &= \begin{cases} \rho_1 \left(\frac{\dot{m}}{\dot{m}_0}\right) \left(\frac{r}{r_f}\right)^{-3/2} & \text{if } r_i < r < r_{\text{tra}}, \\ \rho_2 \left(\frac{\dot{m}}{\dot{m}_0}\right)^{-2} \left(\frac{r}{r_f}\right)^{3/2} & \text{if } r_{\text{tra}} < r < r_{\text{out}}, \end{cases} \end{aligned} \quad (9)$$

where

$$\begin{aligned} k_1 &= r_f \left(\frac{t_1}{t_f}\right)^{38(1-s)/21}, \quad k_2 = r_f \left(\frac{t_1}{t_f}\right)^{38/21}, \quad k_3 = r_f \left(\frac{t_1}{t_f}\right)^{8/21}, \\ T_1 &= T_0, \quad T_2 = T_0 \left(\frac{t_1}{t_f}\right)^{1/4} \left(\frac{r_f}{\dot{m}_0}\right)^{1/4}, \quad \rho_1 = \rho_0, \quad \rho_2 = \rho_0 \left(\frac{r_f}{\dot{m}_0}\right)^3, \\ t_{\text{gas}} &= t_f [281 \cdot \left(\frac{\alpha m}{0.1}\right)^{2/21} \left(\frac{k_2^{16/21}}{k_3}\right)]^{147/170}. \end{aligned} \quad (10)$$

When $t \geq t_{\text{gas}}$, the thin disk region continues advancing inwards. In the outermost region, electron scattering opacity is gradually replaced by free-free absorption. Since the

outer region is now dominated by gas pressure, the kinetic viscosity should be described by $\nu \propto R^{3/5}$ accordingly (Shen & Matzner 2012), and hence its accretion rate $\propto t^{-19/14}$. Similarly the formulae describing the disk evolution can be derived to be,

$$\begin{aligned}
 r_{\text{out}}(t) &= k_4 \left(\frac{t}{t_f} \right)^{5/7}, \\
 \dot{m}(r, t) &= \begin{cases} j_1 \left(\frac{t}{t_f} \right)^{-19(1-s)/14} \left(\frac{r}{r_f} \right)^s & \text{if } r_i < r < r_{\text{tra}}, \\ k_5 \left(\frac{t}{t_f} \right)^{-19/14} & \text{if } r_{\text{tra}} < r < r_{\text{out}}, \end{cases} \\
 T(r, t) &= \begin{cases} T_1 \left(\frac{\dot{m}}{\dot{m}_0} \right)^{1/4} \left(\frac{r}{r_f} \right)^{-5/8} & \text{if } r_i < r < r_{\text{tra}}, \\ T_2 \left(\frac{r}{r_f} \right)^{-3/4} & \text{if } r_{\text{tra}} < r < r_{\text{gas}}, \\ T_3 \left(\frac{\dot{m}}{\dot{m}_0} \right)^{2/5} \left(\frac{r}{r_f} \right)^{-9/10} & \text{if } r_{\text{gas}} < r < r_{\text{ff}}, \\ T_4 \left(\frac{\dot{m}}{\dot{m}_0} \right)^{3/10} \left(\frac{r}{r_f} \right)^{-3/4} & \text{if } r_{\text{ff}} < r < r_{\text{out}}, \end{cases} \\
 \rho(r, t) &= \begin{cases} \rho_1 \left(\frac{\dot{m}}{\dot{m}_0} \right) \left(\frac{r}{r_f} \right)^{-3/2} & \text{if } r_i < r < r_{\text{tra}}, \\ \rho_2 \left(\frac{\dot{m}}{\dot{m}_0} \right)^{-2} \left(\frac{r}{r_f} \right)^{3/2} & \text{if } r_{\text{tra}} < r < r_{\text{gas}}, \\ \rho_3 \left(\frac{\dot{m}}{\dot{m}_0} \right)^{2/5} \left(\frac{r}{r_f} \right)^{-33/20} & \text{if } r_{\text{gas}} < r < r_{\text{ff}}, \\ \rho_4 \left(\frac{\dot{m}}{\dot{m}_0} \right)^{11/20} \left(\frac{r}{r_f} \right)^{-15/8} & \text{if } r_{\text{ff}} < r < r_{\text{out}}, \end{cases} \quad (11)
 \end{aligned}$$

where the boundary r_{ff} separates the region dominated by electron scattering from that by free-free absorption (Shakura & Sunyaev 1973),

$$r_{\text{ff}} \simeq 1.5 \times 10^4 \dot{m}^{2/3}, \quad (12)$$

and

$$\begin{aligned}
 j_1 &= k_1 \left(\frac{t_{\text{gas}}}{t_f} \right)^{3(1-s)/14}, \quad k_4 = k_3 \left(\frac{t_{\text{gas}}}{t_f} \right)^{-3/7}, \quad k_5 = k_2 \left(\frac{t_{\text{gas}}}{t_f} \right)^{3/14}, \\
 T_3 &= T_2 [281 \left(\frac{\alpha m}{0.1} \right)^{2/21} \left(\frac{\dot{m}_0^{16/21}}{r_f} \right)]^{3/20} \left(\frac{\dot{m}_0}{k_2} \right)^{2/7} \left(\frac{t_{\text{gas}}}{t_f} \right)^{16/49}, \\
 \rho_3 &= \rho_2 [281 \left(\frac{\alpha m}{0.1} \right)^{2/21} \left(\frac{\dot{m}_0^{16/21}}{r_f} \right)]^{63/20}, \\
 T_4 &= T_3 (1.5 \times 10^4 \cdot \frac{\dot{m}_0^{2/3}}{r_f})^{-3/20}, \quad \rho_4 = \rho_3 (1.5 \times 10^4 \cdot \frac{\dot{m}_0^{2/3}}{r_f})^{9/40}. \quad (13)
 \end{aligned}$$

Here ρ_4 and T_4 are derived from the continuity of the density and temperature in the outer disk at the time $t_{\text{ff}} = t_f (1.5 \times 10^4 \cdot k_5^{2/3} / k_4)^{21/34}$ (i.e., when the opacity of the outermost region begins to be dominated by free-free absorption, $r_{\text{ff}} = r_{\text{out}}$), respectively. When $t_{\text{gas}} \leq t < t_{\text{ff}}$, the entire disk is composed of an inner, slim disk region, an intermediate, thin disk region dominated by radiation pressure, and an outer, thin disk region dominated by gas pressure plus electron scattering opacity. When $t \geq t_{\text{ff}}$, an additional, thin disk region, supported by gas pressure plus free-free absorption opacity, appears in the outermost disk region.

Phase 2 terminates when the inner, slim disk region is entirely replaced by a thin disk, i.e., $r_{\text{tra}} = r_{\text{i}}$, corresponding to the time

$$t_2 = t_{\text{f}} \left(\frac{k_5}{r_{\text{i}}} \right)^{14/19}. \quad (14)$$

In phase 3, the whole disk is optically thick and geometrically thin, i.e., radiative cooling becomes efficient everywhere. The disk comprises an inner region supported by radiation pressure plus electron scattering opacity, a middle region by gas pressure plus electron scattering opacity and an outer region by gas pressure plus free-free absorption opacity. The evolutionary functions in this phase are same as in Eq. (11) with $r > r_{\text{tra}}$.

Phase 4 begins when ADAF appears in the inner disk region, or the transition radius r_{ADAF} between ADAF and the thin disk region equals r_{i} . ADAF forms when radiation cooling becomes inefficient so that the heat retained in the accretion flow is mostly advected onto the central compact star. Besides the high mass accretion rate in the case of slim disks, here the very low density of the gas can also inhibit cooling when the accretion rate reaches a few percent of the Eddington accretion rate. The magnitude of r_{ADAF} is somewhat uncertain. It has been empirically deduced from the observations of X-ray binaries and super massive black holes in other galaxies to be (Yuan & Narayan 2004; Cao & Wang 2014),

$$r_{\text{ADAF}} \simeq \dot{m}^{-1/2}, \quad (15)$$

from which the end time of phase 3 is obtained to be

$$t_3 = (k_5 r_{\text{i}}^2)^{14/19} t_{\text{f}}. \quad (16)$$

Similar as in the slim disk case, we assume that there are outflows accompanied with ADAF, thus $\dot{m} \propto r^p$ (Blandford & Begelman 1999). Based on Eq. (15) and the evolution of \dot{m} in the thin disk region, $\dot{m}(r) \propto t^{-19/14}$, the accretion rate in the ADAF region can be written as

$$\dot{m}(r, t) = j_2 \left(\frac{t}{t_{\text{f}}} \right)^{-19(1+p/2)/14} \left(\frac{r}{r_{\text{f}}} \right)^p, \quad (17)$$

where

$$j_2 = r_{\text{f}}^p k_5^{1+p/2}. \quad (18)$$

During the whole evolution, the temperature of the disk keeps decreasing. One can work out the time t_{crit} , at which the disk starts to experience thermal-viscous instability, by

equating the accretion rate with the critical accretion rate for different chemical compositions (most likely He, C or O; [Menou et al. 2002](#)),

$$\begin{aligned}\dot{m}_{\text{crit}}^{\text{He}}(r) &= 5.74 \times 10^{-14} (\alpha/0.1)^{0.41} m^{0.75} r^{2.62}, \\ \dot{m}_{\text{crit}}^{\text{C}}(r) &= 7.39 \times 10^{-13} (\alpha/0.1)^{0.44} m^{0.49} r^{2.23}, \\ \dot{m}_{\text{crit}}^{\text{O}}(r) &= 1.86 \times 10^{-11} (\alpha/0.1)^{0.45} m^{0.37} r^{2.05}.\end{aligned}\tag{19}$$

In the above derivations, we simply assume that the disk can expand all the way. Actually both self-gravity and the neutral process can pose strong constraints on the outer radius and hence the disk evolution. If $r_{\text{sg}} < r_{\text{out}}$, the disk will be truncated by self-gravity. Meanwhile, the disk becomes neutral when the local temperature is very low. This yields the neutral radius r_{neu} where $T(r_{\text{neu}}) = T_{\text{p}}$. The outer radius of an active disk should not be beyond either r_{sg} or r_{neu} . So we have

$$r_{\text{out}} = \begin{cases} r_{\text{out}} & \text{if } r_{\text{out}} < r_{\text{sg}} \ \& \ r_{\text{neu}}, \\ \min(r_{\text{sg}}, r_{\text{neu}}) & \text{if } r_{\text{out}} \geq r_{\text{sg}}, r_{\text{neu}}.\end{cases}\tag{20}$$

Note that in the presence of disk winds, the magnitude of the accretion rate critically depends on the outer boundary. The corresponding evolutionary functions are worked out and presented in the Appendix A and B. In the following, we present the numerically calculated results with different input parameters.

3. Numerical results

For simplicity here we assume that the Shakura & Sunyaev viscosity parameter is invariant (i.e., $\alpha = 0.1$), and the power-law indices related to wind loss are same, i.e., $p = s$. By changing the initial parameters we construct several models, and allocate a name for each model with four parameters (η , t_{f} , r_{i} and r_{f}), where r_{i} actually does not appear unless $r_{\text{i}} \neq 2.5$, neither does r_{f} unless $r_{\text{f}} \neq 1000$. For example, the name $\eta 0.1 t_{\text{f}} 0.5 r_{\text{i}} 6$ denotes the model parameters of $\eta = 0.1$, $t_{\text{f}} = 0.5$ s, $r_{\text{i}} = 6$, and $r_{\text{f}} = 1000$.

According to Eqs. (1), (3), (9) and (11), the self-gravity radius (r_{sg}) is a piecewise continuous function with three turning points at $t = t_1$, t_{gas} and t_{ff} . Once r_{sg} begins to be less than the outer radius (r_{out}), r_{out} will follow the evolution of r_{sg} . Therefore, depending on the evolutionary parameters at these stages ($t_{\text{f}} < t < t_1$, $t_1 < t < t_{\text{gas}}$, $t_{\text{gas}} < t < t_{\text{ff}}$, $t > t_{\text{ff}}$), the occurrence of the self-gravity truncation (i.e., the time point when $r_{\text{out}} = r_{\text{sg}}$) should be estimated beforehand. Based on the stage when the self-gravity truncation takes place for the first time (see Appendix A for details), the evolution of the disks with different wind loss index can be figured out.

We regard model $\eta 0.1 t_f 0.5$ as our reference model. Based on the estimation of the time t_{sg} when the self-gravity truncation first occurs, we can predict the evolution of the disks with any wind loss index (s). In the model, if the wind loss index satisfies $0.19 \lesssim s \lesssim 0.4$, neutralization acts in the outer disk radius before self-gravity. In Fig. 1, the top panels demonstrate the characteristic radii in the disks, i.e., the outer disk radius (r_{out}), the self-gravity radius (r_{sg}), the neutralization radius (r_{neu}), the transition radii between the slim and thin disk regions (r_{tra}), and between ADAF and the thin disk regions (r_{ADAF}), as a function of time with two typical values of $s = 0$ and 0.34 . The dotted horizontal line denotes the inner radius (r_{i}). Here the effects of the self-gravity truncation and neutral process are clearly demonstrated. While self-gravity tries to truncate the disk, the neutral process limits the outer disk radius within the self-gravity radius. In order to illustrate the variations of the disk structure in the four phases, we show the evolution of the accretion rates at the inner and outer edge (denoted as $\dot{m}(r_{\text{i}})$ and $\dot{m}(r_{\text{out}})$, respectively) in the lower panels of Fig. 1 (note that in Shen & Matzner (2012) only $\dot{m}(r_{\text{i}})$ is plotted). The solid line and the green dot-dashed line denote $\dot{m}(r_{\text{out}})$ and $\dot{m}(r_{\text{i}})$, respectively, which obviously evolve in different ways. As seen from the figure, the duration of a slim disk (phase 1) is less than $0.01 - 0.1$ yr, during which the accretion rate is very high (super-Eddington). In the following $\sim 10^2 - 10^5$ yr (phase 2, see also Fig. 3), the decrease in the accretion rate leads to the development of a thin disk starting at the outer region. Subsequently the entire disk becomes thin, and this phase (phase 3) lasts for about $10^3 - 10^6$ yr, until the inner region starts to become ADAF. The ADAF then develops outwards in phase 4.

Figure 2 shows the evolution of $r_{\text{out}}(t)$, $\dot{m}(r_{\text{out}}, t)$ and $\dot{m}(r_{\text{i}}, t)$ with different s values. In the case of weak (strong) disk wind, status transitions occur earlier (later) with increasing s (see the top panel). This feature is caused by the evolution of $\dot{m}(r_{\text{out}})$, $T(r_{\text{out}})$ and $\rho(r_{\text{out}})$ in phase 1, which determines the beginning time of the subsequent phase. For weak or strong wind, $\dot{m}(r_{\text{out}}) \propto t^{-(4+s)/3}$ or $\propto t^{(2s-5)/3}$, so larger s means a faster or slower decrease of \dot{m} with time, and a faster or slower status transition, respectively (see also Fig. 3).

An important phenomenon in the evolution is the occurrence of thermal instability in the disk. The upper panel of Fig. 3 describes how the critical timescales (t_{crit}) evolve with s by comparing the accretion rate at r_{out} with the critical accretion rate for the disk instability with different chemical compositions (He, C and O). Since the time for the disk to be unstable is very short ($\lesssim 20$ yr), the accreting NS should be observed as a very bright, persistent source only for a short time, then quickly becomes a transient source with its peak luminosity decreasing with time.

Figure 4 compares the evolution of the accretion rates $\dot{m}(r_{\text{out}})$ and $\dot{m}(r_{\text{i}})$, the outer disk radius r_{out} , and the three times t_{crit} , t_2 and t_3 with different values of t_f and η . Obviously the

larger η , the longer the times for status-transition (i.e., t_{crit} , t_2 and t_3), irrespective of s , and the outer disk radius is more likely to be truncated by self-gravity. Similarly, the longer t_f , usually the later the status-transitions and neutralization. In addition, the times discussed here all have a minimum at $s \simeq 1/3$, which is caused by the \dot{m} evolution in phase 1.

Finally we examine how the evolution changes with r_i and r_f . We find that, except $\dot{m}(r_i, t)$, neither $r_{\text{out}}(t)$ nor $\dot{m}(r_{\text{out}}, t)$ displays significant changes with the variation in r_i . The effect of the variations in r_f manifests in the evolution of r_{out} , i.e., the disk is more easily truncated by self-gravity with a larger r_f .

4. Discussion

Although there is no direct observational evidence of the WD merger/AIC events, our calculations can be used to predict some possible observational features of the post-AIC systems. The newborn NS may firstly be observed as a super-Eddington persistent X-ray source, and quickly evolve to be transient within $\lesssim 100$ yr. Then the transient source becomes fainter, and its peak X-ray luminosity during outbursts is expected to decrease with time, until the disk becomes passive. Considering the evolution of the mass accretion rate, the post-AIC system tends to spend a very long time as a faint transient source. Here the transient event originates from a similar physical process to that in low-mass X-ray binaries (LMXBs), which occurs once the accretion rate is lower than a critical value (e.g., [Lasota 2001](#)). These features may strongly constrain the models involving fossil disk accretion onto NSs, for example, those for anomalous X-ray pulsars and soft γ -ray repeaters (e.g., [Alpar 2001](#); [Ertan et al. 2009](#)).

A large fraction of LMXBs are transient. They spend most of their lifetime at quiescence with very low X-ray luminosities of $L_X \sim 10^{31-34} \text{ erg s}^{-1}$, and are occasionally active during outbursts with peak luminosities $L_X \sim 10^{36-39} \text{ erg s}^{-1}$ (in the 2-10 keV band). The typical duty cycle (DC) is $\lesssim 10\%$ (e.g., [Chen et al. 1997](#); [Williams et al. 2006](#)). Their transient behavior can be explained with the thermal-viscous instability in the accretion disk irradiated by the X-ray radiation from the central compact object, which causes the disk to transit between a cold-neutral state and a hot-ionized state ([Lasota 2001](#)).

In the last decade a new type of X-ray transients called very faint X-ray transients (VFXTs) were discovered. Their most striking feature is that the 2 – 10 keV luminosities during outbursts ($\sim 10^{34-36} \text{ erg s}^{-1}$) are at least 10 – 100 lower than those of normal X-ray transients (e.g., [Sakano et al. 2005](#); [Muno et al. 2005b](#); [Degenaar & Wijnands 2009](#); [Degenaar](#)

et al. 2012)². However, this classification sensitively depends on the distance determinations of the sources (Armas Padilla et al. 2014). In addition there are hybrid systems displaying both normal and very faint outbursts (Wijnands et al. 2002; Munro et al. 2003; Degenaar & Wijnands 2009; Del Santo et al. 2010; Degenaar & Wijnands 2010).

A large fraction of known VFXTs are very close to Sgr A* (within 10', e.g., Munro et al. 2005b; Porquet 2005; Wijnands et al. 2006; Degenaar & Wijnands 2009) and only a handful sources are observed far from it (Hands et al. 2004; Heinke et al. 2009, 2010; Bozzo et al. 2011), which might be due to the preferred high-resolution X-ray observations in the Galactic center (Degenaar & Wijnands 2009). Most known VFXTs exhibit high Galactic absorption, with only two exceptions (M15 X-3 and Swift J1357.2-0933, Heinke et al. 2009; Armas Padilla et al. 2013). The optical companions of most VFXTs must be fainter than B2 V stars, since no infrared or optical counterparts with a magnitude of $K < 15$ have so far been detected (Munro et al. 2005b; Mauerhan et al. 2009; Degenaar et al. 2012).

The vast majority of VFXTs are likely to be accreting NS and BH systems since only one accreting WD has exhibited outbursts with peak luminosities above $10^{34} \text{ erg s}^{-1}$ (i.e., GK Per, Watson et al. 1985). Observations of VFXTs suggest that they should comprise some heterogeneous populations (e.g., Munro et al. 2005b; Sakano et al. 2005; King & Wijnands 2006; Degenaar & Wijnands 2009; Armas Padilla et al. 2011; Degenaar et al. 2012). By analogy with the normal transients, if the typical radiation-efficiency of accretion ($\sim 10^{20} \text{ erg/g}$) and DC ($\lesssim 10\%$) are applied to VFXTs, the long-term time-averaged accretion rate $\langle \dot{M} \rangle$ should be $\lesssim 10^{-13} - 10^{-12} M_{\odot} \text{ yr}^{-1}$ (King & Wijnands 2006; Heinke et al. 2015). LMXBs with such low \dot{M} can hardly evolve from the traditional Roche-lobe overflow (RLOF) process within Hubble time, unless some abrupt change of \dot{M} occurs (e.g., Maccarone & Patruno 2013).

King & Wijnands (2006) proposed that part of the VFXTs may be LMXBs harboring either an extremely low-mass companion (such as a brown dwarf or a planet) or an intermediate-mass BH to guarantee that the average mass transfer rate is extremely low, but the birth rates of such systems are highly uncertain.

The propeller effect of a NS accretor may also lead to a particularly low accretion rate (Degenaar & Wijnands 2009; Heinke et al. 2009; Armas Padilla et al. 2011). Accretion onto a NS can be inhibited by the centrifugal barrier unless its spin angular velocity is smaller than

²Some bright accretion-disk-corona (ADC) sources appear very faint if observed at a large orbital-inclination angle (e.g., Munro et al. 2005a; Wijnands et al. 2006). Statistical analysis shows that this kind of sources should contribute a small amount of VFXTs rather than the bulk, so the sub-luminous outbursts are intrinsic (King & Wijnands 2006; Degenaar et al. 2012).

the Keplerian angular velocity at the magnetosphere (Illarionov & Sunyaev 1975). Numerical simulations show that diffusive and viscous interaction between the magnetosphere and the disk may play an important role in the propeller-driven outflows and there is always a slow accretion flow in the case of weak-propeller systems (Romanova et al. 2004, 2005). Based on this picture, Degenaar et al. (2014) tried to explain the very faint persistent outburst of XMM J174457–2850.3. This model can be tested by future measurements of the spin and the magnetic field of the accreting NS.

Here we suggest that an accreting NS (formed via WD merger) from a fossil disk may account for part of the VFXT population, considering the fact that $\gtrsim 1/3$ VFXTs are NS systems and the optical counterparts, if exist, are either very faint or undetectable. Whether the merger remnant can evolve into a VFXT depends on the evolution of the fossil disk, provided that the NS has a weak magnetic field ($< 10^{10}$ G). The key points are whether the disk can be thermally unstable and maintain a very low accretion rate $\lesssim 10^{-12} M_{\odot} \text{ yr}^{-1}$ for a sufficiently long time. The time when the system reaches such low accretion rate is an increasing function of the initial disk mass (or its formation timescale), and is estimated to be $\gtrsim 10^5$ yr from our previous calculations.

Population synthesis calculations (e.g., Chen et al. 2012) show that the Galactic birthrate of NSs born via double WD mergers is about $5 \times 10^{-4} \text{ yr}^{-1}$. Adopting a lifetime of $\gtrsim 10^5$ yr, we can then roughly estimate that there might be $\gtrsim 100$ transient NSs accreting from a fossil disk, with the properties resembling VFXTs. For such objects, some observational features can distinguish them from those in LMXBs:

- (i) No orbital modulations would be displayed in its light curve since there is not any companion star.
- (ii) One may expect to detect spectral lines from C or O elements in the disk.
- (iii) The delay time for WD mergers can be as short as a few 10^8 yr (Chen et al. 2012), so WD mergers may trace the star-formation processes. This may partly explain why there are a rich population of VFXTs in the Galactic center region.

5. Conclusions

AIC is expected to be an important channel to the formation of MSPs theoretically (e.g., Hurley et al. 2010), although direct observational evidence is still lacking. In this paper we investigate the evolution of the merger remnant of double WDs (i.e., a fossil disk around a NS), taking into account the effect of the outer radius, which is determined by

either self-gravity or neutralization.

We find that the evolution generally consists of four phases. (i) In phase 1, the newborn fossil disk is a slim one, and accretes onto the NS at a super-Eddington rate. As a consequence, the system should be observed as a very bright persistent source. However, the duration of the phase is less than 1 yr. (ii) In phase 2, the slim disk gradually evolves to be a thin disk with the decrease of the accretion rate, since radiative cooling becomes effective. The transition starts from the outer region and develops inwards until the entire disk turns into a thin disk (within a time $\sim 10^{1-6}$ yr). During the evolution, the disk is expected to be thermally unstable within $\lesssim 100$ yr, i.e., the system changes to a bright transient X-ray source, and the peak X-ray luminosity decreases with time. The outer disk either is truncated by self-gravity or becomes neutral and stops spreading any more. (iii) In phase 3 the whole disk is a thin disk. The evolution of the thin disk can last $\sim 10^{2-7}$ yr, during which the X-ray brightness of the transient source becomes even lower. (iv) In phase 4, the thin disk turns into an ADAF from the inner region once the accretion rate decrease to $\lesssim 0.01\dot{M}_{\text{Edd}}$, where advective cooling is dominated.

During the disk evolution, we consider possible wind loss since the accretion rate can be significantly higher or lower than \dot{M}_{Edd} (Blandford & Begelman 1999; Narayan et al. 2001). In our calculations, the outer radius of the disk is firstly determined. Based on the estimation, the evolution of the disk with different wind loss indices can then be predicted. One can estimate when the disk evolves from a slim disk to a thin disk, and when the NS evolves from persistent to transient, depending on the self-gravity truncation or the neutral process. On one hand, the disk will spread more slowly if truncated by the self-gravity. On the other hand, the self-gravity truncation tends to postpone the occurrence of the neutralization.

Based on the calculations, a possible picture of the fossil disk accretion onto an isolated NS is predicted. Unlike previous studies on the early evolution of the fallback disk, here we are interested in the evolution of the post-AIC systems at the late phase, during which the source appears faint ($L_X < 10^{36}$ erg s $^{-1}$). Indeed, ~ 40 peculiar transients, called VFXTs, have been captured by the high-resolution monitors during the past decade (e.g., King & Wijnands 2006; Degenaar & Wijnands 2009; Degenaar et al. 2012). Our calculations demonstrate that the post-AIC systems may be transient within 100 yr and reach a very low accretion rate of $10^{-12} M_{\odot} \text{ yr}^{-1}$ at a time $\gtrsim 10^5$ yr, implying that the post-AIC systems could be the progenitors of some VFXTs.

We are grateful to an anonymous for clarifying and helpful comments. This work was supported by the Natural Science Foundation of China under grant numbers 11133001 and 11333004, and the Strategic Priority Research Program of CAS (under grant number

XDB09000000).

If both the self-gravity truncation and the neutral process are considered, the disk evolution will behave differently, and will be described in the appendix. For simplification, the density (ρ_i , $i=0, 1, 2, 3, 4$) in the following discussions is assumed to be nondimensional.

A. Disk Evolution with self-gravity truncation

Since the disk in each phase follows the distinct evolution (Section 2.2), the self-gravity truncation can hardly be described by a common function. If there is self-gravity truncation, we assume that $r_{\text{out}} = r_{\text{sg}}$ is satisfied unless there is a new state-transition. Depending on the initial parameters, self-gravity truncation can occur at any stage. In addition, if the wind loss index satisfies $s \rightarrow 1$, the outer region will be easily truncated.

Moreover, the disk may be truncated at the beginning of phase 1 under specific situations. Firstly, a timescale t_{sg0} when $r_{\text{out}} = r_{\text{sg}}$, using the evolutionary parameters in phase 1, is calculated to be,

$$t_{\text{sg0}} = \begin{cases} t_f \cdot \left(\frac{2.92 \times 10^5}{r_f \cdot \rho_0^{1/3} \cdot m^{2/3}} \right)^{-9/(1+s)} & (0 < s < 1/3), \\ t_f \cdot \left(\frac{2.92 \times 10^5}{r_f \cdot \rho_0^{1/3} \cdot m^{2/3}} \right)^{-9/(2-2s)} & (1/3 < s < 1), \end{cases} \quad (\text{A1})$$

From Eq. (3), one can infer that increase of r_{sg} with time ($\sim \propto t^{7/9}$, $0 < s < 1$) is faster than that of r_{out} with time ($\propto t^{2/3}$). Then the disk evolution should be described by $r_{\text{out}} = r_{\text{sg}}$ from the time point of t_f to that of $t = \min(t_{\text{sg0}}, t_1)$. In the following, we only consider models with $t_{\text{sg0}} \leq t_f$. Depending on the occurrence of self-gravity truncation, the disk evolution can be classified as follows.

(i) If the disk is truncated at $t_1 < t < t_{\text{gas}}$, the outer radius evolves in the following laws,

$$r_{\text{out}}(t_1 < t < t_{\text{sg}}) = k_3 \cdot \left(\frac{t}{t_f} \right)^{2/7}, \quad (\text{A2})$$

$$r_{\text{out}}(t_{\text{sg}} < t < t_{\text{gas}}) = r_f \cdot \left(\frac{2.92 \times 10^5}{r_f \cdot \rho_2^{1/3} \cdot m^{2/3}} \right)^{2/3} \cdot \left(\frac{k_2}{\dot{m}_0} \right)^{4/9} \cdot \left(\frac{t}{t_f} \right)^{-32/63}, \quad (\text{A3})$$

where

$$t_{\text{sg}} = t_f \cdot \left(\frac{r_f}{k_3} \right)^{63/50} \cdot \left(\frac{2.92 \times 10^5}{r_f \cdot \rho_2^{1/3} \cdot m^{2/3}} \right)^{21/25} \cdot \left(\frac{k_2}{\dot{m}_0} \right)^{14/25},$$

$$t_{\text{gas}} = t_f \cdot \left[\frac{281}{r_f} \cdot (m\alpha/0.1)^{2/21} \cdot k_2^{16/21} \cdot \left(\frac{\dot{m}_0}{k_2} \right)^{4/9} \cdot \left(\frac{r_f \cdot \rho_2^{1/3} \cdot m^{2/3}}{2.92 \times 10^5} \right)^{2/3} \right]^{441/160}. \quad (\text{A4})$$

When $t_{\text{gas}} < t < t_{\text{ff}}$, we have

$$\begin{aligned} r_{\text{out}}(t_{\text{gas}} < t < t_{\text{ff}}) &= r_{\text{f}} \cdot \left(\frac{2.92 \times 10^5}{r_{\text{f}} \cdot \rho_3^{1/3} \cdot m^{2/3}} \right)^{20/9} \cdot \left(\frac{k_5}{\dot{m}_0} \right)^{-8/27} \cdot \left(\frac{t}{t_{\text{f}}} \right)^{76/189}, \\ r_{\text{out}}(t > t_{\text{ff}}) &= r_{\text{f}} \cdot \left(\frac{2.92 \times 10^5}{r_{\text{f}} \cdot \rho_4^{1/3} \cdot m^{2/3}} \right)^{8/3} \cdot \left(\frac{k_5}{\dot{m}_0} \right)^{-22/45} \cdot \left(\frac{t}{t_{\text{f}}} \right)^{209/315}, \end{aligned} \quad (\text{A5})$$

where

$$t_{\text{ff}} = t_{\text{f}} \cdot \left[\frac{1.5 \times 10^4}{r_{\text{f}}} \cdot \dot{m}_0^{2/3} \cdot \left(\frac{k_5}{\dot{m}_0} \right)^{26/27} \cdot \left(\frac{r_{\text{f}} \cdot \rho_3^{1/3} \cdot m^{2/3}}{2.92 \times 10^5} \right)^{20/9} \right]^{189/247}, \quad (\text{A6})$$

and some other parameters are referred to Eq. (11)–(18).

(ii) If self-gravity truncation occurs at $t_{\text{gas}} < t < t_{\text{ff}}$, the evolution of the outer radius follows,

$$\begin{aligned} r_{\text{out}}(t_{\text{gas}} < t < t_{\text{sg}}) &= k_4 \cdot \left(\frac{t}{t_{\text{f}}} \right)^{5/7}, \\ r_{\text{out}}(t_{\text{sg}} < t < t_{\text{ff}}) &= r_{\text{f}} \cdot \left(\frac{2.92 \times 10^5}{r_{\text{f}} \cdot \rho_3^{1/3} \cdot m^{2/3}} \right)^{20/9} \cdot \left(\frac{k_5}{\dot{m}_0} \right)^{-8/27} \cdot \left(\frac{t}{t_{\text{f}}} \right)^{76/189}, \end{aligned} \quad (\text{A7})$$

where

$$t_{\text{sg}} = t_{\text{f}} \cdot \left[\frac{r_{\text{f}}}{k_4} \cdot \left(\frac{2.92 \times 10^5}{r_{\text{f}} \cdot \rho_3^{1/3} \cdot m^{2/3}} \right)^{20/9} \cdot \left(\frac{k_5}{\dot{m}_0} \right)^{-8/27} \right]^{189/59}. \quad (\text{A8})$$

The evolution after t_{ff} can be described by Eq. (A5) and (A6).

(iii) In other cases the evolution of the outer radius is given by

$$\begin{aligned} r_{\text{out}}(t_{\text{ff}} < t < t_{\text{sg}}) &= k_4 \cdot \left(\frac{t}{t_{\text{f}}} \right)^{5/7}, \\ r_{\text{out}}(t > t_{\text{sg}}) &= r_{\text{f}} \cdot \left(\frac{2.92 \times 10^5}{r_{\text{f}} \cdot \rho_4^{1/3} \cdot m^{2/3}} \right)^{8/3} \cdot \left(\frac{k_5}{\dot{m}_0} \right)^{-22/45} \cdot \left(\frac{t}{t_{\text{f}}} \right)^{209/315}, \end{aligned} \quad (\text{A9})$$

where

$$t_{\text{sg}} = t_{\text{f}} \cdot \left[\frac{r_{\text{f}}}{k_4} \cdot \left(\frac{2.92 \times 10^5}{r_{\text{f}} \cdot \rho_4^{1/3} \cdot m^{2/3}} \right)^{8/3} \cdot \left(\frac{k_5}{\dot{m}_0} \right)^{-22/45} \right]^{315/16}, \quad (\text{A10})$$

and the following evolution is similar to that described by case (i).

B. Disk Evolution with Neutralization

In the above calculations, the effect of the neutral process is ignored. According to our calculations, the time (t_{neu}) for the outer disk to become neutral satisfies $t_2 > t_{\text{neu}} > t_{\text{ff}}$. Thus, when $t > t_{\text{neu}}$, the disk is composed of a hot region ($r_{\text{i}} < r < r_{\text{neu}}$) and a cold region $r_{\text{neu}} < r < r_{\text{out}}$, where

$$r_{\text{neu}}(t) = r_{\text{f}} \cdot \left(\frac{T_4}{300 \text{ K}}\right)^{4/3} \cdot \left(\frac{k_5}{\dot{m}_0}\right)^{2/5} \cdot \left(\frac{t}{t_{\text{f}}}\right)^{-19/35}. \quad (\text{B1})$$

And the neutralization time t_{neu} can be calculated from the condition $r_{\text{neu}} = r_{\text{out}}$, i.e.,

$$t_{\text{neu}} = \begin{cases} t_{\text{f}} \cdot \left(\frac{T_4}{300 \text{ K}}\right)^{21/19} \cdot \left(\frac{k_5 \cdot \rho_4}{\dot{m}_0}\right)^{14/19} \cdot \left(\frac{2.92 \times 10^5}{r_{\text{f}} \cdot \dot{m}^{2/3}}\right)^{-42/19} & (t_{\text{neu}} > t_{\text{sg}}), \\ t_{\text{f}} \cdot \left(\frac{T_4}{300 \text{ K}}\right)^{35/33} \cdot \left(\frac{k_5}{\dot{m}_0}\right)^{7/22} \cdot \left(\frac{k_4}{r_{\text{f}}}\right)^{-35/44} & (\text{otherwise}), \end{cases} \quad (\text{B2})$$

where r_{out} is described by Eq. (A9), based on whether the outer region has been truncated or not before being neutral. Substituting Eq. (B2) into Eq. (B1), one can obtain the maximal r_{out} , $r_{\text{out,max}} = r_{\text{neu}}(t_{\text{neu}})$.

REFERENCES

- Abramowicz, M. A., Czerny, B., Lasota, J. P., & Szuszkiewicz, E. 1988, *ApJ*, 332, 646
- Aggarwal, H. R., & Oberbeck, V. R. 1974, *ApJ*, 191, 577
- Alpar, M. A. 2001, *ApJ*, 554, 1245
- Alpar, M. A., Çalışkan, Ş., & Ertan, Ü. 2013, *IAUS*, 290, 93
- Armas Padilla, M., Degenaar, N., Patruno, A., Russell, D. M., Linares, M., Maccarone, T. J., Homan, J., & Wijnands, R. 2011, *MNRAS*, 417, 659
- Armas Padilla, M., Degenaar, N., Russell, D. M., & Wijnands, R. 2013, *MNRAS*, 428, 3083
- Armas Padilla, M., Wijnands, R., Degenaar, N., et al. 2014, *MNRAS*, 444, 902
- Benz, W., Bowers, R. L., Cameron, A. G. W., & Press, W. H. 1990, *ApJ*, 348, 647
- Bhattacharya, D., & van den Heuvel, E. P. J. 1991, *Phys. Rep.*, 203, 1
- Blandford, R. D., & Begelman, M. C. 1999, *MNRAS*, 303, L1
- Bozzo, E., Ferrigno, C., Stevens, J., Belloni, T. M., Rodriguez, J., den Hartog, P. R., Papitto, A., et al. 2011, *AA*, 535, L1
- Burderi, L., King, A. R., & Szuszkiewicz, E. 1998, *ApJ*, 509, 85
- Cannizzo, J. K., & Gehrels, N. 2009, *ApJ*, 700, 1047
- Cannizzo, J. K., Lee, H. M., & Goodman, J. 1990, *ApJ*, 351, 38
- Cao, X., & Wang, J.-X. 2014, *arXiv*: 1406.6442
- Chen, X., Jeffery, C. S., Zhang, X., & Han, Z., 2012, *ApJL*, 755, L9
- Chen, W., Shrader, C. R., & Livio, M. 1997, *ApJ*, 491, 312
- Chevalier, R. A. 1989, *ApJ*, 346, 847
- Dan, M., Rosswog, S., Guillochon, J., & Ramirez-Ruiz, E. 2011, *ApJ*, 737, 89
- Darbha, S., Metzger, B. D., Quataert, E., Kasen, D., Nugent, P., & Thomas, R. 2010, *MNRAS*, 409, 846
- Degenaar, N., & Wijnands, R. 2009, *AA*, 495, 547

- Degenaar, N., & Wijnands, R. 2010, AA, 524, A69
- Degenaar, N., Wijnands, R., Cackett, E. M., Homan, J., in't Zand, J. J. M., Kuulkers, E., et al. 2012, AA, 545, 49
- Degenaar, N., Wijnands, R., Reynolds, M. T., Miller, J. M., & Altamirano, D. 2014, ApJ, 792, 109
- Del Santo, M., Sidoli, L., Romano, P., Bazzano, A., Wijnands, R., Degenaar, N., & Mereghetti, S. 2010, MNRAS, 403, L89
- Dessart, L., Burrows, A., Livne, E., & Ott, C. D. 2007, ApJ, 669, 585
- Dessart, L., Burrows, A., Ott, C. D., Livne, E., Yoon, S.-Y., & Langer, N. 2006, ApJ, 644, 1063
- D'Souza, M. C. R., Motl, P. M., Tohline, J. E., & Frank, J. 2006, ApJ, 643, 381
- Duncan, R. C., & Thompson, C. 1992, ApJ, 392, L9
- Ertan Ü., Ekşi, K. Y., Erkut, M. H., & Alpar, M. A. 2009, ApJ, 702, 1309
- Fryer, C. L., Holz, D. E., & Hughes, S. A. 2002, ApJ, 565, 430
- García-Berro, E., et al. 2012, ApJ, 749, 25
- García-Berro, E., Lorén-Aguilar, P., Pedemonte, A. G., Isern, J., et al. 2007, ApJ, 661, L179
- Hands, A. D. P., Warwick, R. S., Watson, M. G., & Helfand, D. J. 2004, MNRAS, 351, 31
- Han, Z., Podsiadlowski Ph., Maxted, P. F. L., Marsh, T. R., & Ivanova, N. 2002, MNRAS, 336, 449
- Heber, U. 2009, ARAA, 47, 211
- Heinke, C. O., Altamirano, D., Cohn, H. N., Lugger, P. M., Budac, S. A., Servillat, M., Linares, M., et al. 2010, ApJ, 714, 894
- Heinke, C. O., Bahramian, A., Degenaar, N., & Wijnands, R. 2015, MNRAS, 447, 3034
- Heinke, C. O., Cohn, H. N., & Lugger, P. M. 2009, ApJ, 692, 584
- Holberg, J. B., Sion, E. M., Oswalt, T., McCook, G. P., Foran, S., & Subasavage, J. P. 2008, AJ, 135, 1225

- Hurley, J. R., Tout, C. A., Wickramasinghe, D. T., Ferrario, L., & Kiel, P. D. 2010, MNRAS, 402, 1437
- Iben, I., & Tutukov, A. V. 1984, ApJS, 54, 335
- Illarionov, A. F., & Sunyaev, R. A. 1975, AA, 39, 185
- Inotsuka, S., & Sano, T. 2005, ApJ, 628, L155
- Jeffery, C. S., Karakas, A. I., & Saio, H. 2011, MNRAS, 414, 3599
- Kato, S., Fukue, J., & Mineshige, S. 1998, Black hole accretion disks (Kyoto Univ. Press)
- Kawai, Y., Saio, H., & Nomoto, K. 1987, ApJ, 315, 229
- Külebi, B., Ekşi, K. Y., Lorén-Aguilar, P., Isern, J., & García-Berro, E. 2013, MNRAS, 431, 2778
- Kilic, M., Brown, W. R., Gianninas, A., Hermes, J. J., Allende Prieto, C., & Kenyon, S. J. 2014, MNRASL, 444, L1
- King, A. R., Pringle, J. E., & Wickramasinghe, D. T. 2001, MNRAS, 320, L45
- King, A. R., & Wijnands, R. 2006, MNRAS, 366, L31
- Lasota, J.-P. 2001, New Astron. Rev., 45, 449
- Levan, A. J., Wynn, G. A., Chapman, R., et al. 2006, MNRAS, 368, L1
- Liebert, J., Bergeron, P., & Holberg, J. B. 2005, ApJS, 156, 47
- Longland, R., Lorén-Aguilar, P., José J., García-Berro, E., et al. 2011, ApJL, 737, L34
- Lorén-Aguilar, P., Isern, J., & García-Berro, E. 2009, AA, 500, 1193
- Lynden-Bell, D., & Pringle, J. E. 1974, MNRAS, 168, 603
- Maccarone, T. J., & Patruno, A. 2013, MNRAS, 428, 1335
- Mauerhan, J. C., Munro, M. P., Morris, M. R., et al. 2009, ApJ, 703, 30
- Menou, K., Perna, R., & Hernquist, L. 2001, ApJ, 559, 1032
- Menou, K., Perna, R., & Hernquist, L. 2002, ApJ, 564, L81
- Metzger, B. D., Piro, A. L., & Quataert, E. 2008, MNRAS, 390, 781

- Metzger, B. D., Piro, A. L., & Quataert, E. 2009a, MNRAS, 396, 304
- Metzger, B. D., Piro, A. L., & Quataert, E. 2009b, MNRAS, 396, 1659
- Michel, F. C. 1988, Nat, 333, 644
- Motl, P. M., Frank, J., Tohline, J. E., & D’Souza, M. C. R. 2007, ApJ, 670, 1314
- Muno, M. P., Baganoff, F. K., & Arabadjis, J. S. 2003, ApJ, 598, 474
- Muno, M. P., Lu, J. R., Baganoff, F. K., Brandt, W. N., Garmire, G. P., et al. 2005a, ApJ, 633, 228
- Muno, M. P., Pfahl, E., Baganoff, F. K., Brandt, W. N., Ghez, A., Lu, J., & Morris, M. R. 2005b, ApJ, 622, L113
- Narayan, R., Piran, T., & Kumar, P. 2001, ApJ, 557, 949
- Nomoto, K., & Iben, I. Jr. 1985, ApJ, 297, 531
- Nomoto, K., & Kondo, Y. 1991, ApJ, 367, L19
- Ott, C. D. 2009, Class. Quant. Gravity, 26, 063001
- Phinney, E. S. 1989, in IAU Symp. 136, the Center of the Galaxy, ed. M. Morris (Dordrecht: Kluwer), 543
- Porquet, D., Grosso, N., Burwitz, V., et al. 2005, AA, 430, L9
- Pringle, J. E. 1974, Ph. D. thesis, University of Cambridge
- Pringle, J. E. 1981, ARAA, 19, 137
- Pringle, J. E. 1991, MNRAS, 248, 754
- Raskin, C., & Kasen, D. 2013, ApJ, 772, 1
- Rees, M. J. 1988, Nature, 333, 523
- Romanova, M. M., Ustyugova, G. V., Koldoba, A. V., & Lovelace, R. V. E. 2004, ApJ, 616, L151
- Romanova, M. M., Ustyugova, G. V., Koldoba, A. V., & Lovelace, R. V. E. 2005, ApJ, 635, L165

- Rueda, J. A., Boshkayev, K., Izzo, L., Ruffini, R., Lorén-Aguilar, P., et al. 2013, *ApJL*, 772, L24
- Sadowski, A. 2011, PhD thesis (Nicolaus Copernicus Astronomical Center); arXiv: 1108.0396
- Saio, H., & Jeffery, C. S. 2000, *MNRAS*, 313, 671
- Saio, H., & Nomoto, K. 1985, *AA*, 150, L21
- Saio, H., & Nomoto, K. 1998, *ApJ*, 500, 388
- Saio, H., & Nomoto, K. 2004, *ApJ*, 615, 444
- Sakano, M., Warwick, R. S., Decourchelle, A., & Wang, Q. D. 2005, *MNRAS*, 357, 1211
- Shakura, N. I., & Sunyaev, R. A. 1973, *AA*, 24, 337
- Shen, R.-F., & Matzner, C. D. 2012, in *EPJ Web of Conferences*, Vol. 39, Tidal Disruption Events and AGN Outbursts, ed. R. Saxton & S. Komossa (Madrid, Spain: EPJ Web of Conferences), 07006
- Toomre, A. 1964, *ApJ*, 139, 1217
- Usov, V. V. 1992, *nature*, 357, 472
- van Kerkwijk, M. H. 2013, *Phil. Trans. R. Soc. A*, 371, 20120236
- van Kerkwijk, M. H., Chang, P., & Justham, S. 2010, *ApJL*, 722, L157
- Watarai, K., Fukue, J., & Takeuchi, M. 2000, *PASJ*, 52, 133
- Watson, M. G., King, A. R., & Osborne, J. 1985, *MNRAS*, 212, 917
- Webbink, R. F. 1984, *ApJ*, 277, 355
- Whelan, J., & Iben, I. 1973, *ApJ*, 186, 1007
- Wijnands, R., in’t Zand, J. J. M., Rupen, M., Maccarone, T., Homan, J., Cornelisse, R., Fender, R., et al. 2006, *AA*, 449, 1117
- Wijnands, R., Miller, J. M., & Wang, Q. D. 2002, *ApJ*, 579, 422
- Williams, B. F., Naik, S., Garcia, M. R., & Callanan, P. J. 2006, *ApJ*, 643, 356
- Yoon, S.-C., Podsiadlowski, P., & Rosswog, S. 2007, *MNRAS*, 380, 933

- Yuan, F., & Narayan, R. 2004, *ApJ*, 612, 724
- Yuan, J. W. 1992, *AA*, 261, 105
- Yu, S., & Jeffery, C. S. 2010, *AA*, 521, A85
- Zhang, X., Jeffery, C. S., Chen, X., & Han, Z. 2014, *MNRAS*, 445, 660
- Zhu, C., Chang, P., van Kerkwijk, M. H., & Wadsley, J. 2013, *ApJ*, 767, 164

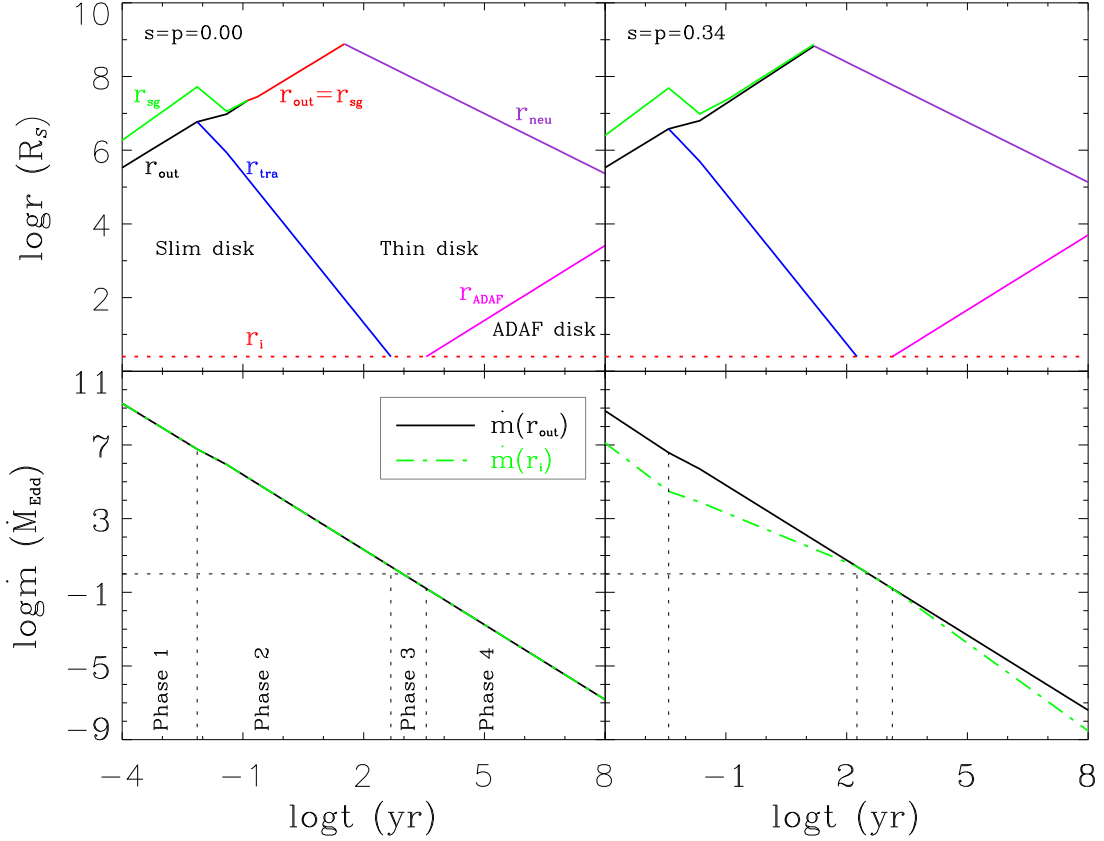


Fig. 1.— Evolution of the disk radii and the accretion rate at the inner region (r_i) and the outermost region (r_{out}) during the four phases in the model $\eta 0.1 t_f 0.5$. Here r_{sg} is the self-gravity radius, r_{neu} is the boundary between the cold disk with temperature of ≤ 300 K and the inner hot disk, r_{tra} is the transition radius between the slim disk and the thin disk, r_{ADAF} detaches the inner ADAF from the outer thin disk.

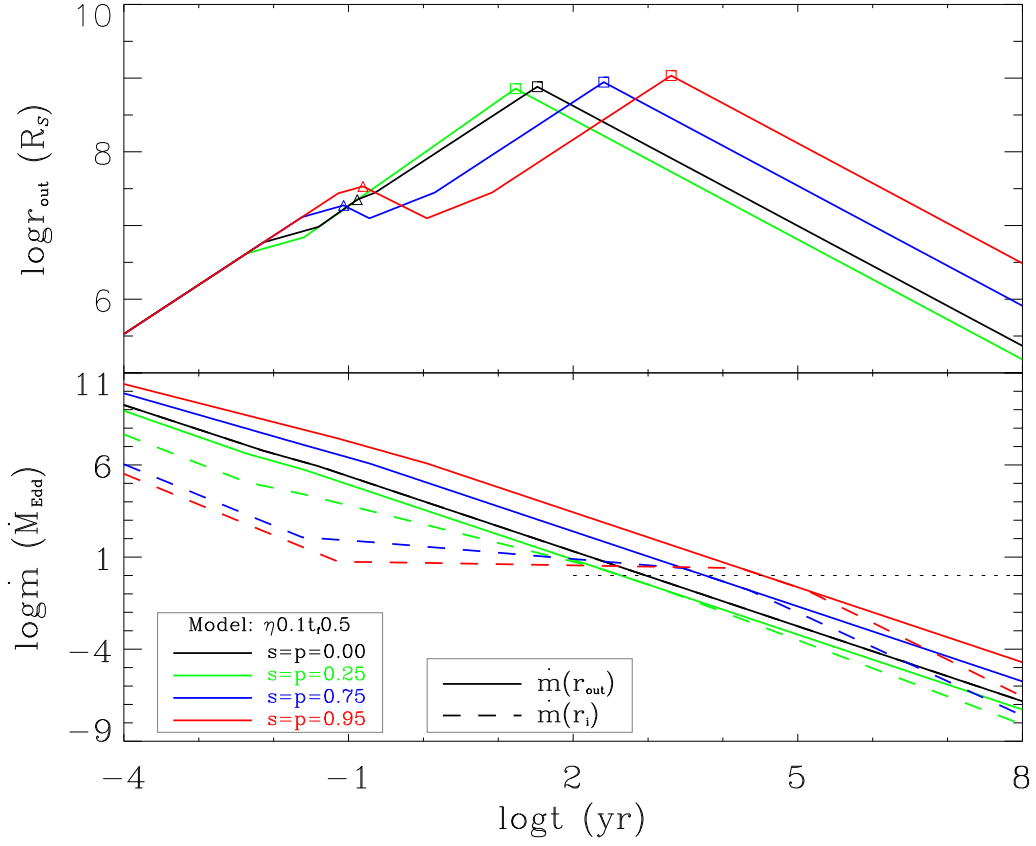


Fig. 2.— Evolution of the outer disk radii and the accretion rate in the model $\eta 0.1 t_{\text{f}} 0.5$, with different values of s . The triangle and rectangle denote the start of self-gravity truncation and neutralization, respectively.

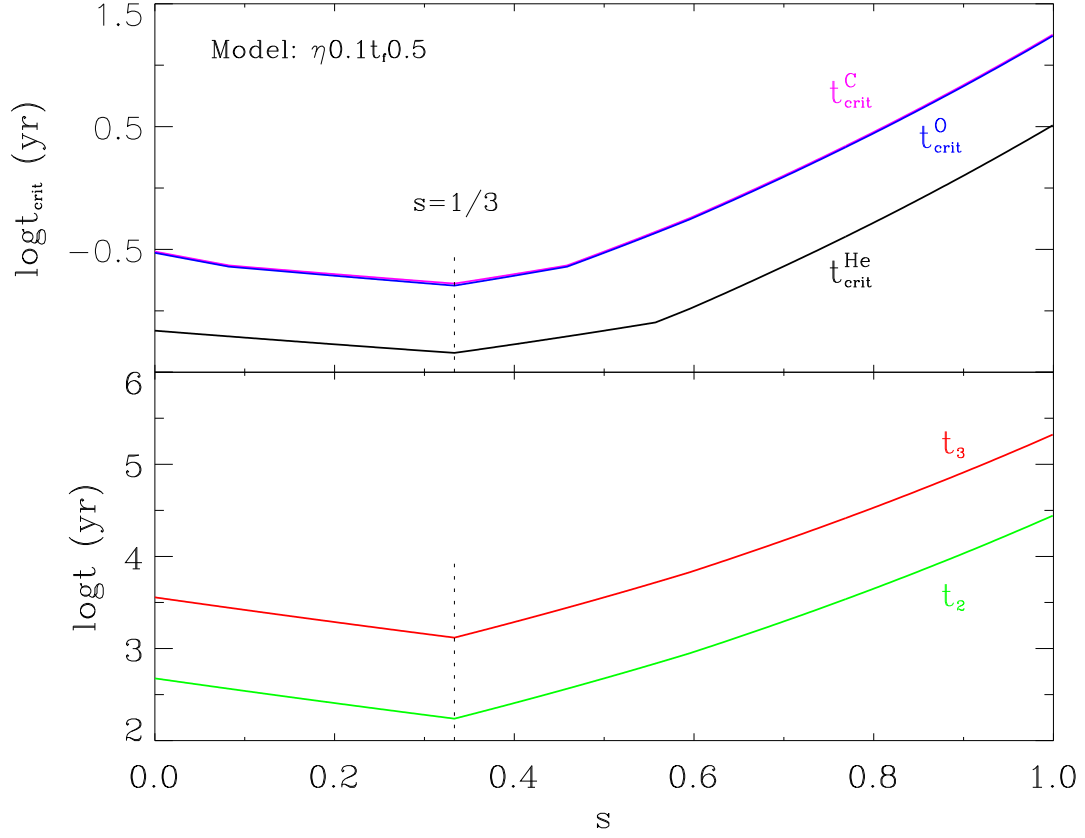


Fig. 3.— The upper panel shows the time when the disk becomes thermally unstable in the model $\eta 0.1 t_f 0.5$ as function of s . The bottom panel shows the times for the whole disk becoming optically thick (t_2) and the appearance of ADAF.

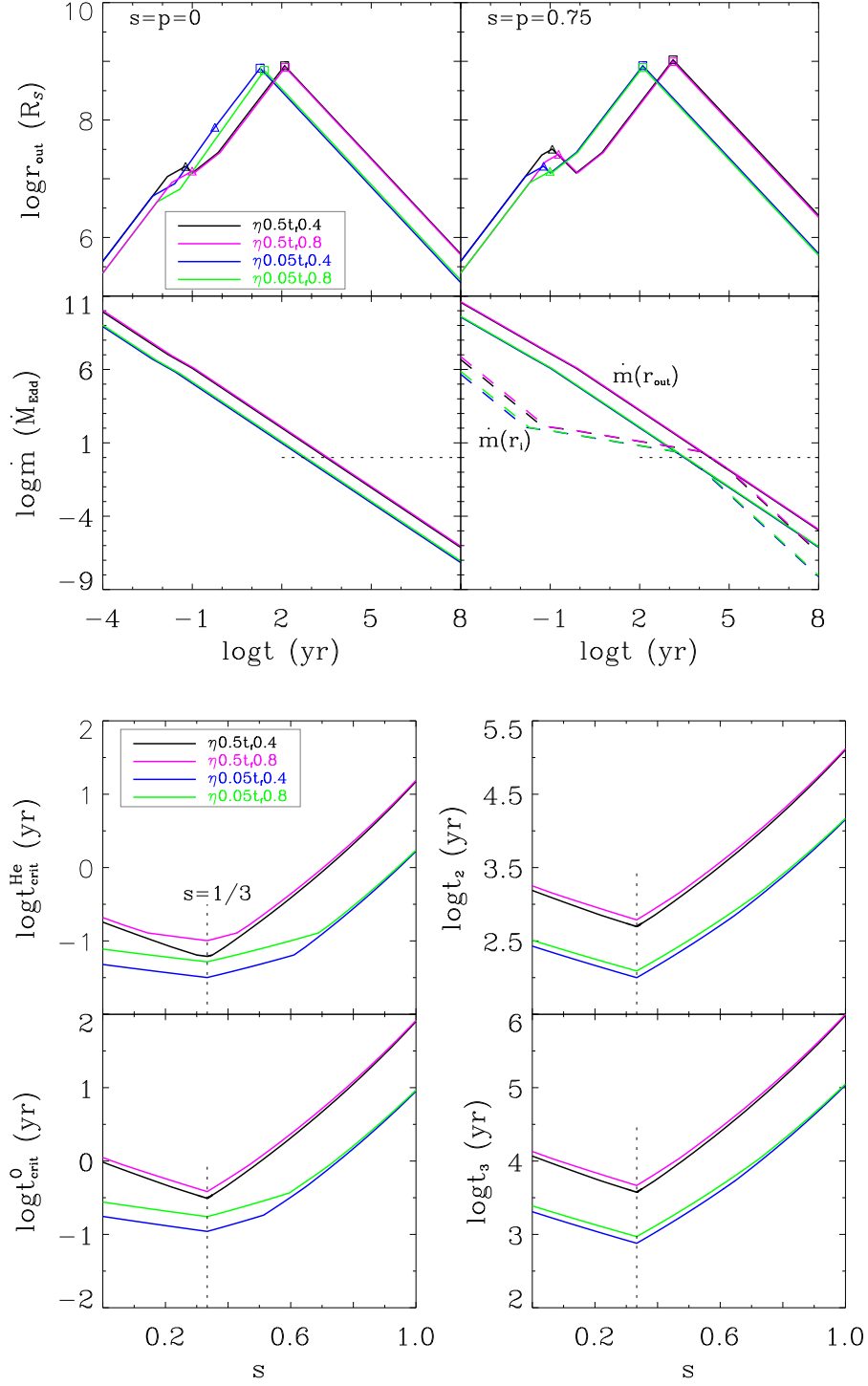


Fig. 4.— Models with different values of η and t_f are compared by simulating the evolution of accretion rate $\dot{m}(r_{\text{out}})$, $\dot{m}(r_i)$, r_{out} , t_{crit} , t_2 , and t_3 . Here four models with $r_i = 2.5$, $r_f = 1000$, as labeled by legends, are considered.